Development of a CT-compatible anthropomorphic skull phantom for surgical planning, training, and simulation

Lai, Marco; Skyrman, Simon; Kor, Flip; Homan, Robert; Babic, Drazenko; Edström, Erik; Persson, Oscar; Burström, Gustav; Elmi-Terander, Adrian; Hendriks, Benno H.W.

DOI
10.1117/12.2577629

Publication date
2021

Document Version
Final published version

Published in
Medical Imaging 2021

Development of a CT-compatible anthropomorphic skull phantom for surgical planning, training, and simulation

Lai, Marco, Skyrman, Simon, Kor, Flip, Homan, Robert, Babic, Drazenko, et al.

Marco Lai, Simon Skyrman, Flip Kor, Robert Homan, Drazenko Babic, Erik Edström, Oscar Persson, Gustav Burström, Adrian Elmi-Terander, Benno H. W. Hendriks, Peter H. N. de With, "Development of a CT-compatible anthropomorphic skull phantom for surgical planning, training, and simulation," Proc. SPIE 11601, Medical Imaging 2021: Imaging Informatics for Healthcare, Research, and Applications, 116010A (15 February 2021); doi: 10.1117/12.2577629

SPIE.

Event: SPIE Medical Imaging, 2021, Online Only

Development of a CT-compatible anthropomorphic skull phantom for surgical planning, training and simulation

Marco Lai[a,b], Simon Skyrman[c], Flip Kor[d], Robert Homan[e], Drazenko Babic[a], Erik Edström[c], Oscar Persson[c], Gustav Burström[c], Adrian Elmi-Terander[c], Benno H. W. Hendriks[a,d], and Peter H. N. de With[b]

[a]Philips Research, Eindhoven, The Netherlands
[b]Dept. E. Eng, Eindhoven University of Technology, Eindhoven, The Netherlands
[c]Department of Neurosurgery, Karolinska University Hospital and Department of Clinical Neuroscience, Karolinska Institutet, Stockholm, Sweden
[d]Dept. of Biomechanical Eng., Delft University of Technology, Delft, The Netherlands
[e]Philips Healthcare, Best, The Netherlands

ABSTRACT

Neurosurgical procedures require high accuracy and skills, so that practical surgical training is a key factor for successful patient outcomes. Neurosurgical training has been traditionally performed on human cadavers, or more recently on simulation models including virtual reality (VR) platforms. However, these methods have several drawbacks, including ethical and practical concerns. Anthropomorphic phantoms could solve most of the issues related to cadaveric models, and are suitable for simulating several neurosurgical procedures. The aim of this study was to design a realistic and CT-compatible anthropomorphic head phantom that could be used for surgical training and simulation, with a specific focus on endo-nasal skull-base surgery and brain biopsy. A head phantom was created by segmenting a Cone Beam Computed Tomography (CBCT) image and a T1-weighted MR image from a cadaver. The skull, which includes a complete structure of the nasal cavity and detailed skull-base anatomy, is 3D printed using PLA with calcium. The brain phantom is produced using a 3D printed mold, casting a mixture of PVA, water and coolant. The radiodensity and mechanical properties of the phantom were tested and adjusted in material choice to mimic real-life conditions. In general, surgeons have a positive attitude in using the phantom. The skull and the eloquent structures at the skull-base, as well as the brain parenchyma were realistically reproduced. The head phantom can be employed for neurosurgical education, training and surgical planning, and can be successfully used for simulating endo-nasal skull-base surgery and brain biopsies.

Keywords: Anthropomorphic phantom, skull phantom, CT compatible phantom, neurosurgical simulation, endo-nasal skull-base surgery, brain biopsy.

1. INTRODUCTION

Neurosurgical procedures require high accuracy and surgical skills that are acquired and continuously maintained in a safe educational environment. Training laboratories are commonly used, where junior doctors can acquire and improve skills, and experienced surgeons may perform pre-operative simulations of complex surgical cases. Traditionally, neurosurgical training has been performed on human cadavers. While this has the advantage of a risk-free training environment and authentic anatomical conditions, it also requires certain facilities, is expensive and raises ethical and legal concerns.[1] Also, patient anatomy is unique for each individual, and surgical planning based on a cadaver may be inappropriate or even misleading. In recent years, there has been a shift towards simulation-based training, including virtual reality (VR) platforms, that allow immediate feedback and performance measurements. However, many simulators lack realistic force and tactile feedback, do not have convincing visualization or allow the use of actual surgical instruments, incurring high associated

Further author information: (Send correspondence to M.L.)
M.L.: E-mail: marco.lai@philips.com

Medical Imaging 2021: Imaging Informatics for Healthcare, Research, and Applications
edited by Thomas M. Deserno, Brian J. Park, Proc. of SPIE Vol. 11601, 116010A
 · doi: 10.1117/12.2577629

costs.[2] The use of anthropomorphic phantoms could solve many issues related to cadaveric or VR models. Pre-operative CT and/or MRI images of the individual patient may be printed to create a phantom that accurately replicates the patient-specific anatomy. Moreover, realistic anthropomorphic and CT-compatible phantoms can be used for initial tests of new innovative technologies, such as navigation systems, prior to conducting costly cadaveric studies. The advancing technology of 3D printing has enabled creating complex anatomical models with the required accuracy and tactile feedback. The most common phantoms are skulls, which are 3D printed in different plastic materials.[3–6] Phantoms have also been created for modelling of vascular structures, including cerebral artery aneurysms[7] and complex internal carotid artery variants.[8] In Ear, Nose and Throat (ENT) surgery, 3D-printed phantoms have been used for testing AR systems in middle ear surgery[9] and for simulation of sinus and nasal cavity surgery, where the nasal cavities were included in the phantoms.[10] For simulating brain biopsies, brain phantoms have been designed to mimic brain tissue and lesions, and placed inside a cadaveric human skull.[11] An anatomically and mechanically realistic brain phantom was proposed by Chen et al.,[12] and was built by using polyvinyl alcohol cryogel (PVAC), a material widely used in medical imaging phantoms for its mechanical similarities to soft tissues. Even though several examples of anthropomorphic phantoms exist, there is no commercially available phantom that is both CT-compatible and meets the requirements for simulation of neurosurgical procedures.

The aim of this study was to design an anatomically realistic and CT-compatible anthropomorphic skull and brain phantom for surgical planning, training and simulation of neurosurgical procedures, with a specific focus on endo-nasal skull-base surgery and brain biopsies.

2. METHOD

2.1 Phantom requirements for realistic surgical simulations

Endo-nasal skull-base surgery offers a minimally-invasive approach to remove tumors of the skull-base, of which pituitary gland tumors are one of the most common types. In clinical practice, surgery is performed through the nasal cavity, using rigid instruments and a rigid endoscope to visualize the surgical field. To design a phantom for realistic simulation of endo-nasal skull-base surgery, several anatomical structures need to be present. The phantom must contain a correct representation of the nasal cavity including nasal turbinates, nasal meatuses, nasal septum, sphenoidal sinus, natural sphenoidal ostia, sphenoid inter-sinus septum and sella turcica, as well as critical neurovascular structures such as the optic nerves, optic chiasm, pituitary gland and carotid arteries. For training of tumor resection, a realistic model of a tumor and characteristic anatomical changes associated with tumor growth, should also be represented.

Brain biopsies are performed to confirm the diagnostic assessment of brain tumors and other pathologies when the diagnosis is uncertain and surgical resection is not feasible or is not the primary option. A small hole is drilled in the skull, after which a biopsy needle is introduced into the brain and samples for tissue diagnosis are collected. The needle is usually navigated from pre-operative CT and/or MR images. To simulate biopsies, ideally, a skull phantom is needed with a brain having similar mechanical and radiological properties to the real brain.

2.2 Computational model

A computational model of the skull and brain phantom was created from a Cone Beam Computed Tomography (CBCT) and a T1-weighted MR image of a cadaver. The images were acquired at the Cincinnati Children's Hospital Medical Center, Ohio, United States. All ethical guidelines for human cadaver studies were followed. Informed consent for body donation for research and educational purposes were given from the donors. The CBCT and MR images were co-registered, and the open source computer software 3D Slicer[13] was used for segmentation. Manual adjustment of the model was performed to verify the presence of all required anatomic features. The CBCT image was used to model the bony structures, including the nasal cavity. The brain, the pituitary gland, optic chiasm and carotid arteries were segmented from a T1-weighted MRI scan, after which the segmented structures were inverted to negative images to create molds for the phantom's structures. Following the guidelines of experienced neurosurgeons, a pituitary tumor is added to the computational model and the anatomical structures segmented from the cadaver were modified in order to simulate the presence of the tumor. A pituitary tumor originates from cells of the pituitary gland and develops into a growing mass that affects the

surrounding tissues. As the tumor grows, sella turcica, the bony structure where the pituitary gland is seated, is enlarged and thinned out. The normal pituitary gland is compressed and the optic nerves and optic chiasm are dislocated upwards. Figure 1 portrays the segmented structures of interest and their modifications.

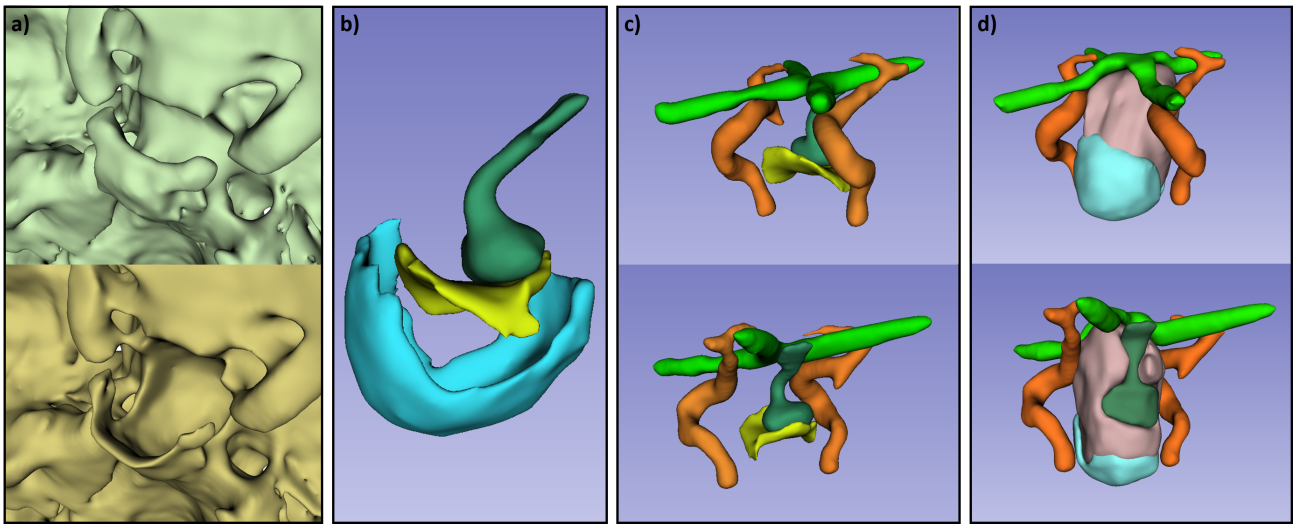

Figure 1. Modifications of the computational model of the cadaveric model. a) Comparison between the original anatomy (top) and the pathological shape of the skull-base (bottom). b) Comparison of the original (yellow) and the enlarged (turquoise) floor of the sella turcica. The original anatomy of the pituitary gland is presented in dark green. c) Anterior and posterior view of the original anatomy of the sella turcica (yellow), internal carotid arteries (orange), optic chiasm (light green) and pituitary gland (dark green). d) Anterior and posterior view of the modified computational model of a pathological condition resulting from a pituitary tumor (blush) with an enlarged sella turcica (turquoise), a compressed pituitary gland (dark green) and a superiorly dislocated optic chiasm (light green).

2.3 Skull phantom

The skull phantom parts were printed using an Ultimaker-3 3D printer (Ultimaker BV, Utrecht, Netherlands). To avoid the need of reprinting, the entire skull with every endonasal surgery simulation, the nasal cavity and frontal skull-base were built as an exchangeable module. Thus, after each simulation, the modular part could be replaced with a new one. The calvarium was designed to be removable to allow placement and replacement of the brain phantom inside the skull phantom (Figure 2). Water-soluble polyvinyl alcohol (PVA) was used as printing support material, and the printed parts were left overnight to let the PVA dissolve, after which they were polished with sandpaper to remove any imperfection. Three materials were considered for building the skull phantom: gypsum powder, PLA (polylactic acid) and PLA+$CaCO_3$[14] (calcium carbonate). Gypsum powder has comparable radiodensity to bone, with Hounsfield Unit (HU) values ranging from 1000 to 3000.[15] PLA is a standard material used for FDM (Fused Deposition Modeling), with properties ideal for 3D printing, but with a radiodensity around 0 HU. By mixing PLA with $CaCO_3$, the HU of the print was increased to approximate the CT attenuation of bone. A CBCT image of each sample was acquired (Philips Healthcare, Best, The Netherlands) and compared to real-bone tissue attenuation, which was acquired from the CBCT examination of the human-skull cadaver. CBCT images were inspected using Matlab.[16] The voxels of the samples' volumes were manually segmented and used for computing the distribution of the attenuation.

2.4 Brain Phantom

The brain phantom was cast in a 3D printed PLA mold that was divided into 8 segments held by a support structure of aluminum, to facilitate ejection of the cast after molding. The big opening at the top of the mold was used to pour in the liquid material, whereas the small one allowed full filling of the mold without leaving air gaps. (Figure 3). The brain tissue model was created using a mixture of water, coolant, polyvinyl alcohol

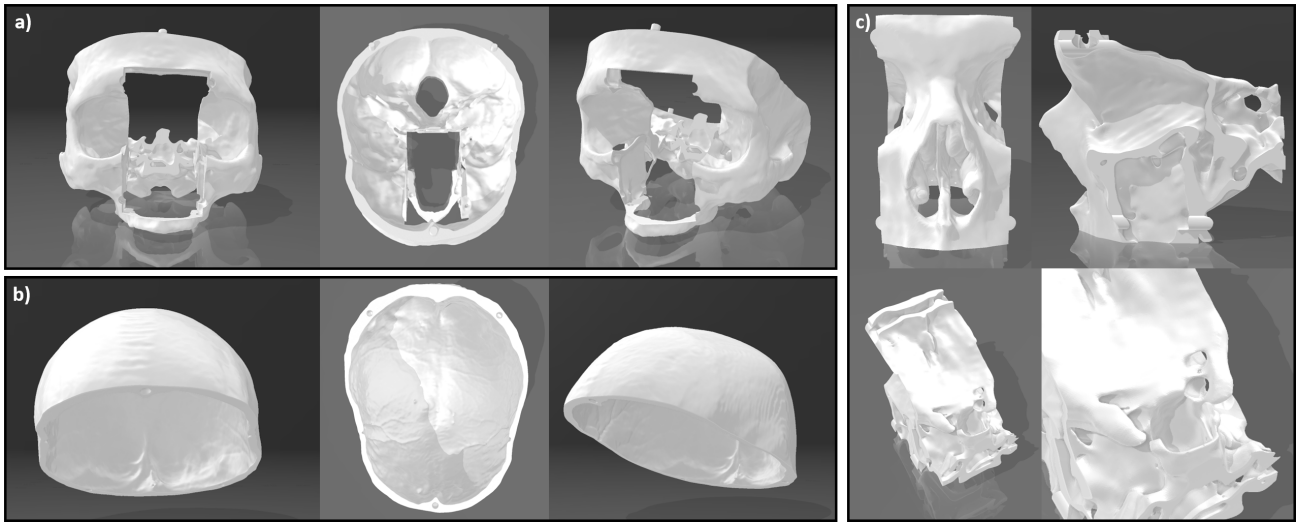

Figure 2. Computational model of the skull segmented from the CBCT image. The computation model of the skull (a) is modified in order to remove the top (b), thus to place the brain inside the skull. The nasal cavity (c) is now modular, thus to be replaced after surgical simulation.

(PVA, Sekisui SELVOL^{TM} Polyvinyl Alcohol 165) and Barium sulfate ($BaSO_4$, SIGMA-ALDRICH ®), using one freeze-thaw cycle at $-25°$ C. The PVA mixture was prepared as previously described by Chen et al.[12] The coolant prevented the 3D printed mold from breaking, due to expansion of the PVA mixture during freezing. The stiffness of the brain phantom material could be controlled by repeated freeze-thaw cycles and/or adjustment of the concentration of PVA. Mechanical properties of several PVA mixtures were tested and compared to brain tissue elasticity. Tested mixtures containing PVA in $wt\%$ (weight percentage) of 3%, 4%, 5%, and 6% were prepared, the rest was water and coolant in a proportion of 60% and 40%, respectively. The PVA samples had a thickness of 20-25 mm and were compressed uniaxially by a linear stage, which exerted its force via a round object with a diameter of 30 mm (contact area of 706.85 mm^2). All tests were carried out at room temperature. The stress-strain curve and elastic modulus of each mixture were measured using a 20-N Force Sensor Xforce-P (Zwick Roell Group, Germany) and compared with the stress-strain response of porcine brain tissue at a strain-rate of 0.01/s, as described by Li et al.[17] To mimic the CT attenuation of brain tissue, Barium sulfate was added to the mixture. A mixture of PVA with water and coolant was prepared. The mixture was split in six samples and Barium sulfate was added to five mixtures in $wt\%$ of 0.1, 0.2, 0.3, 0.4 and 0.5%. One mixture contained no Barium sulfate at all. The radiodensity of the mixtures with different percentages of Barium sulfate were scanned with the CBCT and compared to the attenuation of white and gray matter of real brain tissue. The same approach described for computing the skull-material attenuations was used here.

2.5 Skull-base structures

The models of the pituitary gland, pituitary tumor, the optic nerves, optic chiasm and the internal carotids, were casted in 3D printed resin molds that were designed in two separate pieces, with the dividing line at the axes of the casted structures (Figure 4). The resin material was chosen to allow a high printing accuracy (0.05 mm), since the structures themselves were small (5-30 mm). Several holes were added to let the air leave the mold during casting. Structures were colored by adding a small amount of color ink to the mixture.

3. RESULTS

3.1 Mechanical properties of the brain phantom

In Figure 5, the stress-strain loop responses of the brain phantom samples with compression and decompression cycles are shown. The samples contained PVA concentrations of 3%, 4%, 5% and 6%, respectively. To allow a comparison with the mechanical properties of the porcine brain as described by Li et al.,[17] the elastic modulus

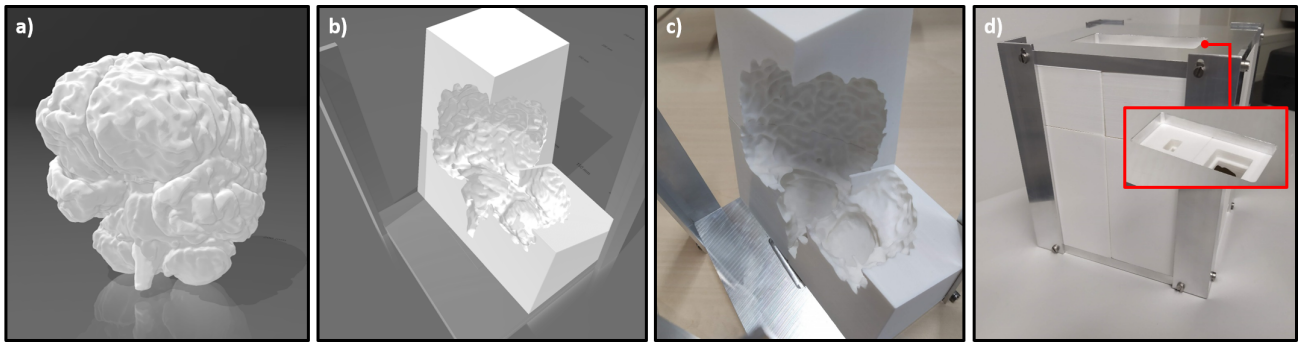

Figure 3. a) Computational model of the brain, segmented from the MR image. b) Inside view of the computational model of the brain mold. c) Inside view of the brain mold. d) Outside view of the brain mold. The red frame shows the big and small openings at the top.

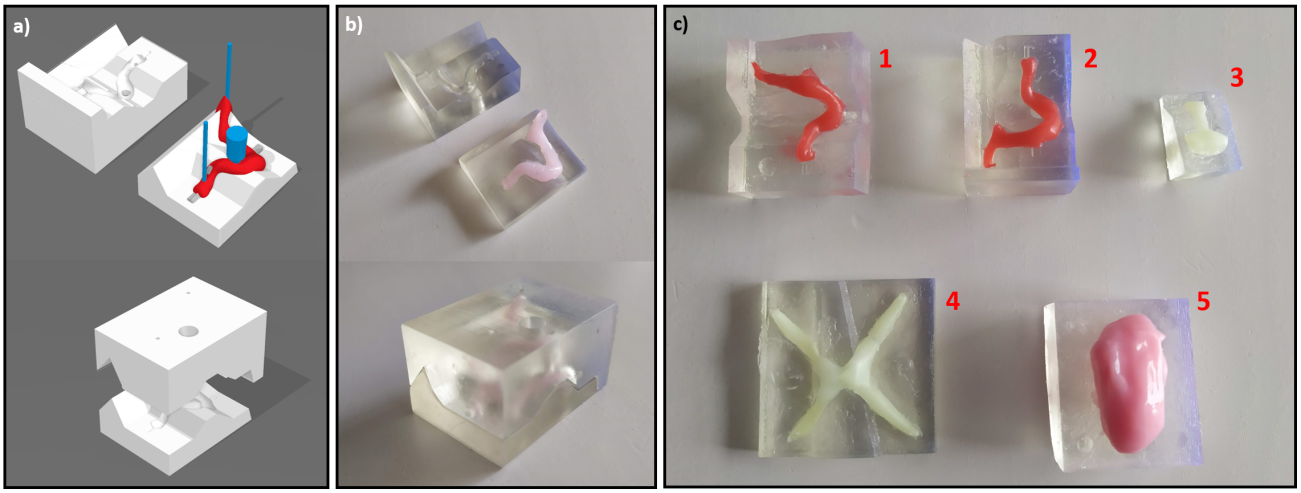

Figure 4. a) Computational model of the mold of one internal carotid. b) Mold of one internal carotid in a resin material. c) Anatomical structures casted with the molds: internal carotids (1, 2), pituitary gland (3), optic nerve (4), tumor (5).

(E) was calculated. The elastic modulus equals the slope of the stress-strain curve, and was calculated for four intervals of the stress-strain curve at 0.01/s. E1 was defined as the elastic modulus for strains of 0-0.1, E2 for strains of 0.1-0.2, E3 for strains of 0.2-0.3 and E4 for strains of 0.3-0.4. The mixture with 4% PVA showed comparable results to porcine brain and was chosen for manufacturing of the brain phantom. Therefore, the final composition of the mixture is 4% PVA and 96% of water and coolant, in proportion of 60% and 40%, respectively.

3.2 Radiodensity of the skull and brain phantom

3.2.1 Radiodensity of the skull phantom

The radiodensity measurements of the materials considered for the skull phantom as well as real bone (skull cadaver) are presented in Figure 6b. PLA had a median value of 3 HU, PLA+$CaCO_3$ of 547 HU and gypsum powered of 955 HU. When choosing material for the skull phantom, ease of production, cost and durability for repeated usage were also considered. Finally the PLA+$CaCO_3$ material was adopted, since it both fulfilled the practical requirements and showed a radiodensity high enough to mimic bone.

3.2.2 Radiodensity of the brain phantom

After testing the mechanical properties of the brain phantom, the experiments on the radiodensity of the brain phantom were carried out with a mixture containing 4% of PVA. The median CT attenuation of the human

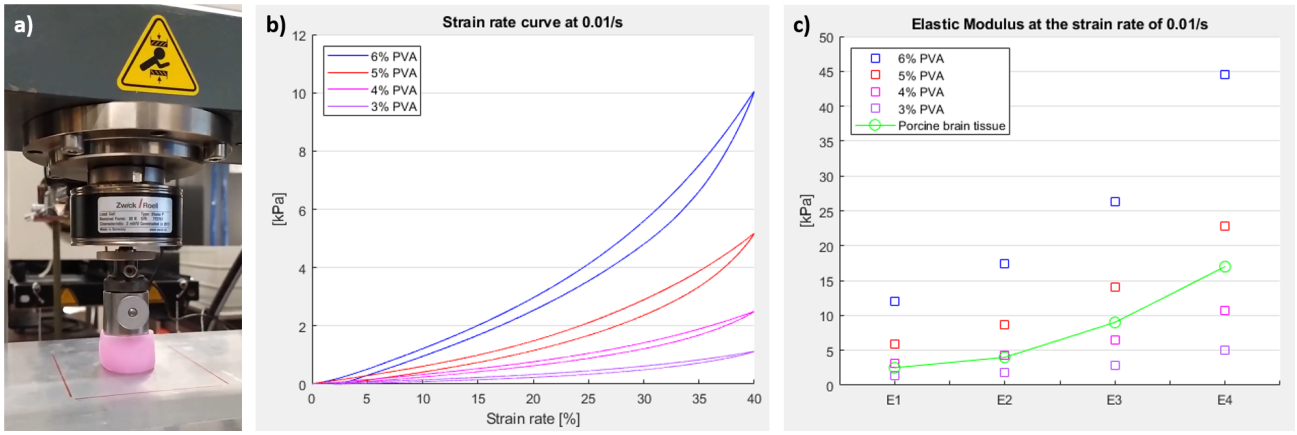

Figure 5. a) PVA sample under test. b) Plotted Strain-rate curves of the mechanical tests on the PVA samples at 0.01/s. c) Elastic moduli of the PVA samples at 0.01/s, compared to the porcine-brain tissue properties found in literature.

brain is approximately 29 HU for white matter and 35 HU for gray matter.[18] Figure 6c shows the radiodensity of the six samples. The PVA-only mixture had a radiodensity of 15 HU. With the addition of Barium sulfate, CT attenuation ranged between 38 HU (0.1% $BaSO_4$) and 136 HU (0.5% $BaSO_4$). The 0.1% $BaSO_4$ mixture had a radiodensity of 38 HU, just slightly higher than gray matter (35 HU), and was chosen as material for the brain phantom.

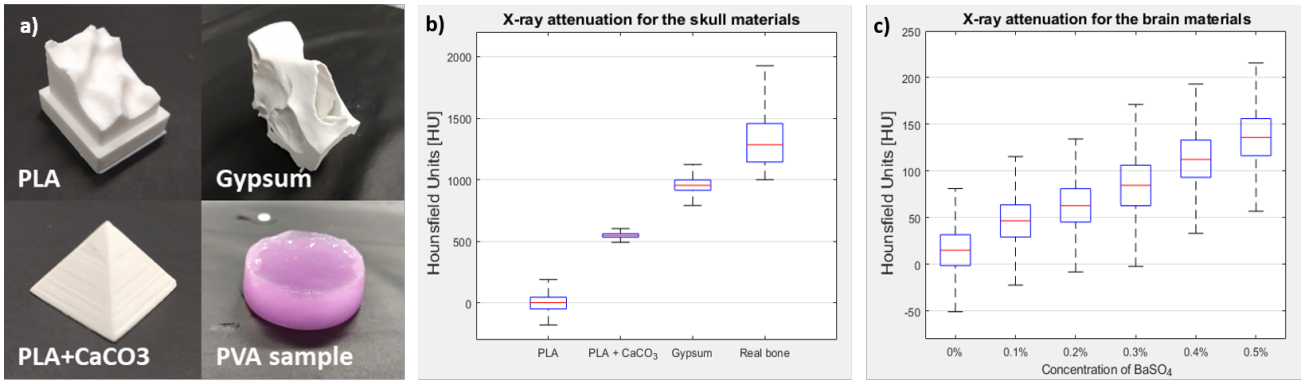

Figure 6. a) Pictures of the X-ray tested materials. b) Boxplots related to the X-ray attenuation, in Hounsfield Units, of the materials for building the skull phantom. c) Boxplots related to the X-ray attenuation, in Hounsfield Units, of the mixtures for producing the brain.

3.3 Final skull and brain phantom

Figure 7 shows the 3D printed head phantom with the skull, the brain and the anatomical structures of the skull-base. The skull can be disassembled into three pieces: the bottom part including the facial skeleton, skull-base and bottom of the calvarium; the top part consisting of the upper part of the calvarium; and the replaceable nasal cavity with the medial frontal skull-base (Figure 7a). The design allows placement and replacement of the brain phantom inside the skull, as well as the nasal cavity, that fits well inside the phantom and stays in position without moving, thanks to the groves on the sides (Figure 7b). Tumor, arteries, nerves and pituitary gland are placed at the base of the skull, on top of the nasal cavity component (Figure 7c, d). The brain fits inside the skull and the anatomical features are well delineated, including the brainstem and the cerebral hemispheres with gyri and sulci present on its entire surface (Figure 7e, f, g, h).

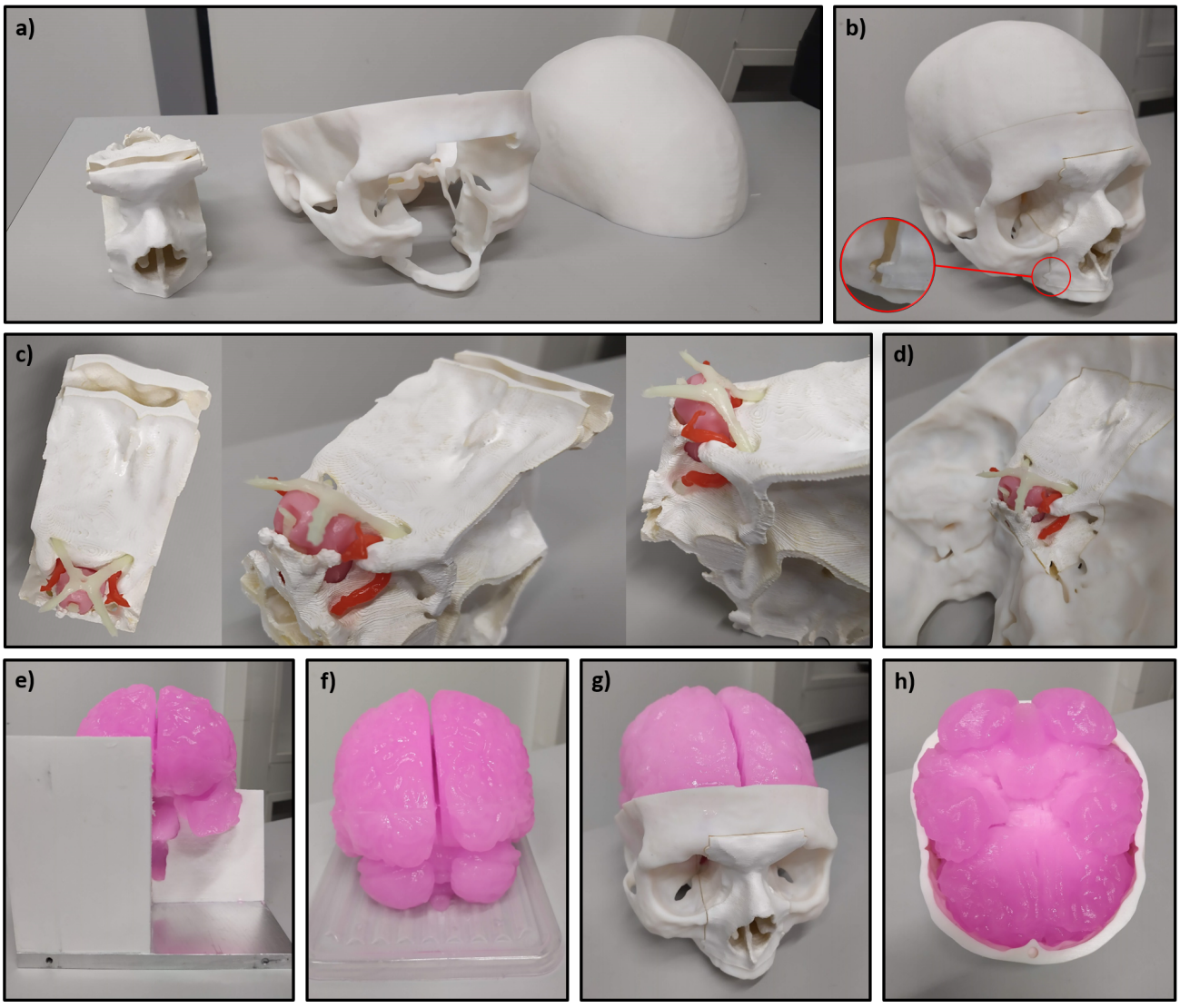

Figure 7. Final head phantom. a) Skull phantom disassembled into its three parts. b) Assembled skull and zoom-in view on the side groove of the maxilla that improves the fitting of the nasal cavity insert into the skull phantom. c) Upper and side views of the nasal cavity and skull-base inserts. d) Back view of the nasal cavity inserted inside the skull. e) Front view of the brain phantom, partially inside the mold. f) Back view of the brain phantom. g) Brain phantom placed inside the skull. h) Brain phantom viewed from below, inserted inside the calvarium of the skull.

4. DISCUSSION

A head phantom was produced, composed of a skull with a removable nasal cavity, critical neurovascular structures at the skull-base, and a brain. Tests of radiodensity and mechanical properties were carried out, in order to produce a phantom with properties as similar as possible to the real skull and brain. Among the three materials tested for the skull bone, PLA, PLA+$CaCO_3$ and gypsum powder, the material chosen for the phantom was PLA+$CaCO_3$. Even though the gypsum powder exhibited a radiodensity closer to bone, the gypsum prints were too fragile and not durable enough for surgical simulations. PLA+$CaCO_3$ was considered a good compromise between radiodensity, ease of production, cost and durability. For the brain phantom, experiments on the PVA samples show that a small amount of $BaSO_4$ suffices to achieve a CT attenuation similar to real brain tissue. Tests were conducted to assess the mechanical properties of the different PVA mixtures. The strain-rate hysteresis loops show that, after compression, some energy is dissipated internally as friction (heat) during the

unloading phase. The 0.01/s curve showed that at lower strains, represented by the elastic moduli E1 and E2, the PVA mixture had a response very similar to real brain. At higher strains, E3 and E4, the sample was stiffer.

The anthropomorphic phantom was evaluated by expert neurosurgeons, who had a positive attitude in using the phantom. The anatomic accuracy and appearance of the skull and nasal cavities were found to be realistic and well designed. Surgeons indicated that a patient-specific head phantom would be useful in surgical planning for cases with complex anatomy. A patient-specific head phantom could improve the surgical planning, since current methods do not always suffice in creating a pre-operative plan. This is because the 2D slices lack depth information and 3D computer imaging may be hard to interpret. However, it should be considered that both the process of segmenting all details of the phantom, as well as the actual 3D printing of the models, are time-consuming. The use of automatic or semi-automatic methods for image segmentation, for example based on deep learning, would improve and speed-up the process.[19]

Surgical simulations using a head phantom may prove to be extremely useful in neurosurgical training, e.g. as a first step for a resident neurosurgeon to use an endoscope in a safe educational environment outside the operation room. The head phantom may be used for practicing techniques that are new to the surgeon, such as the four-hand technique where two surgeons cooperate during the procedure, which is often used during the transsphenoidal approach of pituitary surgery. The head phantom can also be used to mimic the nasal cavities of a patient with abnormal anatomy, where pre-operative training for that specific surgical case would be desired. Furthermore, the phantom can be used for simulating neurosurgical procedures in research and product development.[20,21] The phantom was used for simulation of both skull-base surgery and brain biopsies in research settings. Before going for expensive and cumbersome cadaveric models, navigation technologies can be tested on phantoms with realistic representation of both normal anatomy and pathological conditions. In this way, surgery can be simulated in a safe environment with lower associated costs.[22] Besides the use for pituitary-tumor surgery and brain biopsies, the head phantom would also be interesting for other types of procedures, including removal of brain and skull-base tumors, such as gliomas, meningiomas, chondrosarcomas or chordomas.[23,24] MR and CT images of either patients or cadavers with the mentioned pathologies could be used for creating the phantoms. The anatomical models can also be modified under the guidelines of experienced neurosurgeons to simulate a pathological condition, as we have shown in this paper. The main advantage of this approach is that the computational model of the phantom can serve as a template that can be altered and modified according to the specific pathology, allowing re-use of the basic model for different applications, by slightly altering the anatomy for each case.

5. CONCLUSIONS

In this study, a realistic and CT-compatible anthropomorphic head phantom was designed. The phantom was created using a CBCT and an MR image acquired on a cadaver. In general, surgeons have a positive attitude in using the phantom. The skull and the eloquent structures at the skull-base, as well as the brain parenchyma were realistically reproduced. The head phantom can be employed for neurosurgical education, training and surgical planning, and can be successfully used for simulating endo-nasal skull-base surgery and brain biopsies.

ACKNOWLEDGMENTS

The author Marco Lai has received funding from the European Union's Horizon 2020 research and innovation programme under the Marie Skłodowska-Curie grant agreement No.: 721766 (FBI).

REFERENCES

[1] Breimer, G. E., Bodani, V., Looi, T., and Drake, J. M., "Design and evaluation of a new synthetic brain simulator for endoscopic third ventriculostomy," *Journal of Neurosurgery: Pediatrics* **15**(1), 82–88 (2015).

[2] Lange, T., Indelicato, D. J., and Rosen, J. M., "Virtual reality in surgical training," *Surgical oncology clinics of North America* **9**(1), 61–79 (2000).

[3] Bong, J. H., Song, H.-j., Oh, Y., Park, N., Kim, H., and Park, S., "Endoscopic navigation system with extended field of view using augmented reality technology," *The International Journal of Medical Robotics and Computer Assisted Surgery* **14**(2), e1886 (2018).

[4] Chu, Y., Yang, J., Ma, S., Ai, D., Li, W., Song, H., Li, L., Chen, D., Chen, L., and Wang, Y., "Registration and fusion quantification of augmented reality based nasal endoscopic surgery," *Medical image analysis* **42**, 241–256 (2017).

[5] Gibby, J., Cvetko, S., Javan, R., Parr, R., and Gibby, W., "Use of augmented reality for image-guided spine procedures," *European Spine Journal* **29**(8), 1823–1832 (2020).

[6] Mirota, D. J., Uneri, A., Schafer, S., Nithiananthan, S., Reh, D. D., Gallia, G. L., Taylor, R. H., Hager, G. D., and Siewerdsen, J. H., "High-accuracy 3d image-based registration of endoscopic video to c-arm cone-beam ct for image-guided skull base surgery," in [*Medical Imaging 2011: Visualization, Image-Guided Procedures, and Modeling*], **7964**, 79640J, International Society for Optics and Photonics (2011).

[7] Nagassa, R. G., McMenamin, P. G., Adams, J. W., Quayle, M. R., and Rosenfeld, J. V., "Advanced 3d printed model of middle cerebral artery aneurysms for neurosurgery simulation," *3D printing in medicine* **5**(1), 11 (2019).

[8] Govsa, F., Yagdi, T., Ozer, M. A., Eraslan, C., and Alagoz, A. K., "Building 3d anatomical model of coiling of the internal carotid artery derived from ct angiographic data," *European Archives of Oto-Rhino-Laryngology* **274**(2), 1097–1102 (2017).

[9] Hussain, R., Lalande, A., Marroquin, R., Guigou, C., and Grayeli, A. B., "Video-based augmented reality combining ct-scan and instrument position data to microscope view in middle ear surgery," *Scientific reports* **10**(1), 1–11 (2020).

[10] Narayanan, V., Narayanan, P., Rajagopalan, R., Karuppiah, R., Rahman, Z. A. A., Wormald, P.-J., Van Hasselt, C. A., and Waran, V., "Endoscopic skull base training using 3d printed models with pre-existing pathology," *European Archives of Oto-Rhino-Laryngology* **272**(3), 753–757 (2015).

[11] Cuello, J. F., Saenz, A., Liñares, J. M., Martinez, P., Ruiz, C., Argañaraz, R., Bailez, M. M., and Mantese, B., "Low-cost stereotaxic brain biopsy simulation model," *World Neurosurgery* (2020).

[12] Chen, R. K. and Shih, A., "Multi-modality gellan gum-based tissue-mimicking phantom with targeted mechanical, electrical, and thermal properties," *Physics in Medicine & Biology* **58**(16), 5511 (2013).

[13] Fedorov, A., Beichel, R., Kalpathy-Cramer, J., Finet, J., Fillion-Robin, J.-C., Pujol, S., Bauer, C., Jennings, D., Fennessy, F., Sonka, M., et al., "3d slicer as an image computing platform for the quantitative imaging network," *Magnetic resonance imaging* **30**(9), 1323–1341 (2012).

[14] Filament2Print, "Smartfil ep (ceramic)." https://filament2print.com/gb/wood-ceramic/762-smartfil-ep-limestone.html. Date accessed: January 2021.

[15] Chan, H. H., Siewerdsen, J. H., Vescan, A., Daly, M. J., Prisman, E., and Irish, J. C., "3d rapid prototyping for otolaryngology—head and neck surgery: applications in image-guidance, surgical simulation and patient-specific modeling," *PLoS One* **10**(9), e0136370 (2015).

[16] MATLAB, [*version 9.7.0.1247435 (R2019b)*], The MathWorks Inc., Natick, Massachusetts (2019).

[17] Li, Z., Yang, H., Wang, G., Han, X., and Zhang, S., "Compressive properties and constitutive modeling of different regions of 8-week-old pediatric porcine brain under large strain and wide strain rates," *Journal of the mechanical behavior of biomedical materials* **89**, 122–131 (2019).

[18] Weinstein, M. A., Duchesneau, P. M., and MacIntyre, W. J., "White and gray matter of the brain differentiated by computed tomography," *Radiology* **122**(3), 699–702 (1977).

[19] Akkus, Z., Galimzianova, A., Hoogi, A., Rubin, D. L., and Erickson, B. J., "Deep learning for brain mri segmentation: state of the art and future directions," *Journal of digital imaging* **30**(4), 449–459 (2017).

[20] Lai, M., Shan, C., and de With, P. H., "Hand-eye camera calibration with an optical tracking system," in [*Proceedings of the 12th International Conference on Distributed Smart Cameras*], 1–6 (2018).

[21] Lai, M., Shan, C., Babic, D., Homan, R., Terander, A. E., Edstrom, E., Persson, O., Burstrom, G., et al., "Image fusion on the endoscopic view for endo-nasal skull-base surgery," in [*Medical Imaging 2019: Image-Guided Procedures, Robotic Interventions, and Modeling*], **10951**, 109511D, International Society for Optics and Photonics (2019).

[22] Lai, M., Skyrman, S., Shan, C., Babic, D., Homan, R., Edström, E., Persson, O., Burström, G., Elmi-Terander, A., Hendriks, B. H., et al., "Fusion of augmented reality imaging with the endoscopic view for endonasal skull base surgery; a novel application for surgical navigation based on intraoperative cone beam computed tomography and optical tracking," *Plos one* **15**(1), e0227312 (2020).

[23] Almefty, K., Pravdenkova, S., Colli, B. O., Al-Mefty, O., and Gokden, M., "Chordoma and chondrosarcoma: similar, but quite different, skull base tumors," *Cancer: Interdisciplinary International Journal of the American Cancer Society* **110**(11), 2467–2477 (2007).

[24] Kunimatsu, A. and Kunimatsu, N., "Skull base tumors and tumor-like lesions: a pictorial review," *Polish journal of radiology* **82**, 398 (2017).